applied sciences

MDPI

Article

Quantitative CT Analysis for Predicting the Behavior of Part-Solid Nodules with Solid Components Less than 6 mm: Size, Density and Shape Descriptors

Andrea Borghesi [1,*], Alessandra Scrimieri [1], Silvia Michelini [2], Giulio Calandra [1], Salvatore Golemi [1], Andrea Tironi [3] and Roberto Maroldi [1]

1 Department of Radiology, University and ASST Spedali Civili of Brescia, Piazzale Spedali Civili 1, 25123 Brescia, Italy
2 Department of Radiology, Fondazione Poliambulanza Istituto Ospedaliero, Via Leonida Bissolati 57, 25124 Brescia, Italy
3 Department of Pathology, ASST Spedali Civili of Brescia, Piazzale Spedali Civili 1, 25123 Brescia, Italy
* Correspondence: andrea.borghesi@unibs.it; Tel.: +39-030-395900

Received: 16 July 2019; Accepted: 16 August 2019; Published: 20 August 2019

Abstract: Persistent part-solid nodules (PSNs) with a solid component <6 mm usually represent minimally invasive adenocarcinomas and are significantly less aggressive than PSNs with a solid component ≥6 mm. However, not all PSNs with a small solid component behave in the same way: some nodules exhibit an indolent course, whereas others exhibit more aggressive behavior. Thus, predicting the future behavior of this subtype of PSN remains a complex and fascinating diagnostic challenge. The main purpose of this study was to apply open-source software to investigate which quantitative computed tomography (CT) features may be useful for predicting the behavior of a select group of PSNs. We retrospectively selected 50 patients with a single PSN with a solid component <6 mm and diameter <15 mm. Computerized analysis was performed using ImageJ software for each PSN and various quantitative features were calculated from the baseline CT images. The area, perimeter, mean Feret diameter, linear mass density, circularity and solidity were significantly related to nodule growth ($p \leq 0.031$). Therefore, quantitative CT analysis was helpful for predicting the future behavior of a select group of PSNs with a solid component <6 mm and diameter <15 mm.

Keywords: solitary pulmonary nodule; part-solid nodule; multidetector computed tomography; image processing; computer-assisted; follow-up studies

1. Introduction

Lung nodules represent a common finding on chest computed tomography (CT), and their incidence is steadily increasing [1–3]. With improvements in temporal and spatial resolution, multidetector CT (MDCT) scanners are now able to detect a larger number of nodules, especially small nodules and subsolid nodules (SSNs) [1,3–5].

SSNs, also called ground-glass nodules, are classified as nonsolid or part-solid nodules (PSNs) according to the absence or presence of a solid component within the ground-glass opacity [6,7].

SSNs are a major diagnostic challenge because they may represent a wide variety of malignant and benign lesions [8]. However, when an SSN persists, although the size and density remain unchanged, the likelihood of malignancy is very high, particularly in PSNs [9,10].

Persistent PSNs have a high likelihood of being minimally invasive or invasive adenocarcinomas [7–9]. However, the behavior of PSNs is quite heterogeneous and is related to the size of the nodule and the size of the intralesional solid component [6,7,11]. As a result, in lung cancer screening programs,

the American College of Radiology Lung CT Screening Reporting and Data System (Lung-RADS) guidelines recommend a different follow-up protocol based on the overall size of the nodule and the size of the intralesional solid component [12,13].

In clinical practice, the new Fleischner Society guidelines recommend a first follow-up CT scan at 3–6 months for any PSN ≥6 mm in diameter [6]. Conversely, no routine follow-up CT scan is required for PSN <6 mm in diameter [6]. However, these new guidelines state that only PSNs ≥6 mm in diameter can actually be defined as part-solid [6].

According to the size of the solid component, PSNs can be further categorized as PSNs with a solid component <6 mm and PSNs with a solid component ≥6 mm [6].

PSNs with a solid component <6 mm usually represent minimally invasive adenocarcinomas and are significantly less aggressive than PSNs with a solid component ≥6 mm [6,14]. Therefore, PSNs with a solid component <6 mm could be safely managed with a conservative approach (i.e., annual or biennial follow-up CT scans) [6,14]. Moreover, the "wait and see" approach does not seem to affect the prognosis of patients with PSNs with small solid components [15].

The indications for surgery in PSNs vary according to different guidelines. According to the American College of Chest Physicians, surgical resection is considered for persistent PSNs that range from 8 to 15 mm or for any PSNs >15 mm regardless of their persistence [16]. In contrast, in the new Fleischner Society guidelines, surgical resection is considered only for persistent PSNs with a solid component ≥6 mm in diameter [6]. In addition, some authors recommend surgery only for PSNs with a solid component ≥5 mm or with an overall size ≥15 mm [8].

However, not all PSNs with a small solid component behave in the same way: some nodules exhibit an indolent course, whereas others exhibit more aggressive behavior. Thus, predicting the future behavior of this subtype of PSNs remains a complex and fascinating diagnostic challenge.

Although computerized analyses and various quantitative features have been tested to predict the future behavior of SSNs [9,14,17–22], to our knowledge, there have been no published studies investigating quantitative CT analyses to predict the behavior of PSNs with a solid component <6 mm.

In addition to commercial and in-house image analysis software, several open-source image processing programs have become easily accessible and reliable for performing quantitative analyses on CT images [23].

Therefore, the main purpose of this study was to apply open-source software to investigate which quantitative CT features may be useful for predicting the behavior of a select group of PSNs with a solid component <6 mm and a total diameter <15 mm.

2. Materials and Methods

2.1. Patient and SSN Selection

Through a search on the department radiology information system (RIS) between January 2011 and February 2019, all CT reports containing descriptive terms indicative of persistent SSNs (i.e., nodules unchanged or increased in size at the three-month or longer follow-up CT scan) were retrieved.

The search identified 1157 CT reports with one or more persistent SSNs. The images contained in these CT reports were reviewed by two thoracic radiologists with different levels of experience (A.B. and A.S. with 15 and 4 years of experience, respectively). The study sample was selected according to the following inclusion criteria: (a) solitary PSN with a solid component <6 mm; (b) PSN diameter (i.e., mean between the long axis and short axis on the largest cross-sectional area of the nodule) ≥6 mm and <15 mm; (c) two or more unenhanced chest CT examinations obtained with the same scanner and the same acquisition/reconstruction protocol; (d) thin-section CT images in DICOM format; and (e) no evidence of breathing artifacts on thin-section CT images.

Patients with interstitial lung disease, those who had a recent history of pulmonary infection and those who were undergoing steroid or chemotherapy treatments were excluded.

By applying these criteria, 50 patients with a single PSN with a solid component <6 mm and diameter <15 mm were selected for the present study. The characteristics of the study patients were listed in Table 1.

Table 1. Characteristics of the selected patients (n = 50).

Characteristic	
Age (years)	65.5 ± 10.5
Sex	
Male	24 (48.0)
Female	26 (52.0)
Smoking habits	
Current/former	35 (70.0)
Never	15 (30.0)
Oncologic history	23 (46.0)
Non-small cell lung cancer	10 (43.5)
Breast cancer	4 (17.4)
Head and neck cancer	3 (13.0)
Other malignancy	6 (26.1)

Data are presented as the number (percentage) or mean ± standard deviation.

2.2. CT Acquisition

All chest CT examinations were performed using a 128-slice MDCT scanner (Somatom Definition Flash; Siemens, Germany) with the following parameters: collimation, 128 × 0.6 mm; beam pitch, 1.2; tube voltage, 120 kVp; and tube current-time product, 110 mAs with automatic tube current modulation. The acquisition of the thorax was obtained in inspiratory apnea. All CT data were reconstructed in the axial plane as thin-section (1-mm-thick) images by applying a high-spatial-frequency reconstruction kernel and a lung window setting.

2.3. Computerized Analysis

For each patient, the two thoracic radiologists (A.B. and A.S.) selected thin-section CT images containing the PSNs on the baseline and on the last follow-up CT exam. Before selecting the images, the same observers assessed the lobe location of the PSNs and the absence or presence of emphysema.

Then, the selected CT images were exported in DICOM format, transferred to a personal computer and processed using open-source image processing software (ImageJ software, version 1.52g, U.S. National Institutes of Health, Bethesda, MD, USA, 2018) [24]. The segmentation process and the computerized analysis of PSNs consisted of different steps (Figure 1).

On the baseline CT images, the following quantitative features were considered in the analysis: area, perimeter, mean, median, mode and standard deviation of CT attenuation, skewness, kurtosis and mean Feret diameter (i.e., average between the maximum Feret diameter and the minimum Feret diameter). The maximum Feret diameter corresponded to the longest distance between any two parallel tangents along the nodule contours; in other words, this measure represented the maximum diameter [24–26]. The minimum Feret diameter corresponded to the shortest distance between any two parallel tangents along the nodule contours; in other words, this measure represented the minimum diameter [24–26].

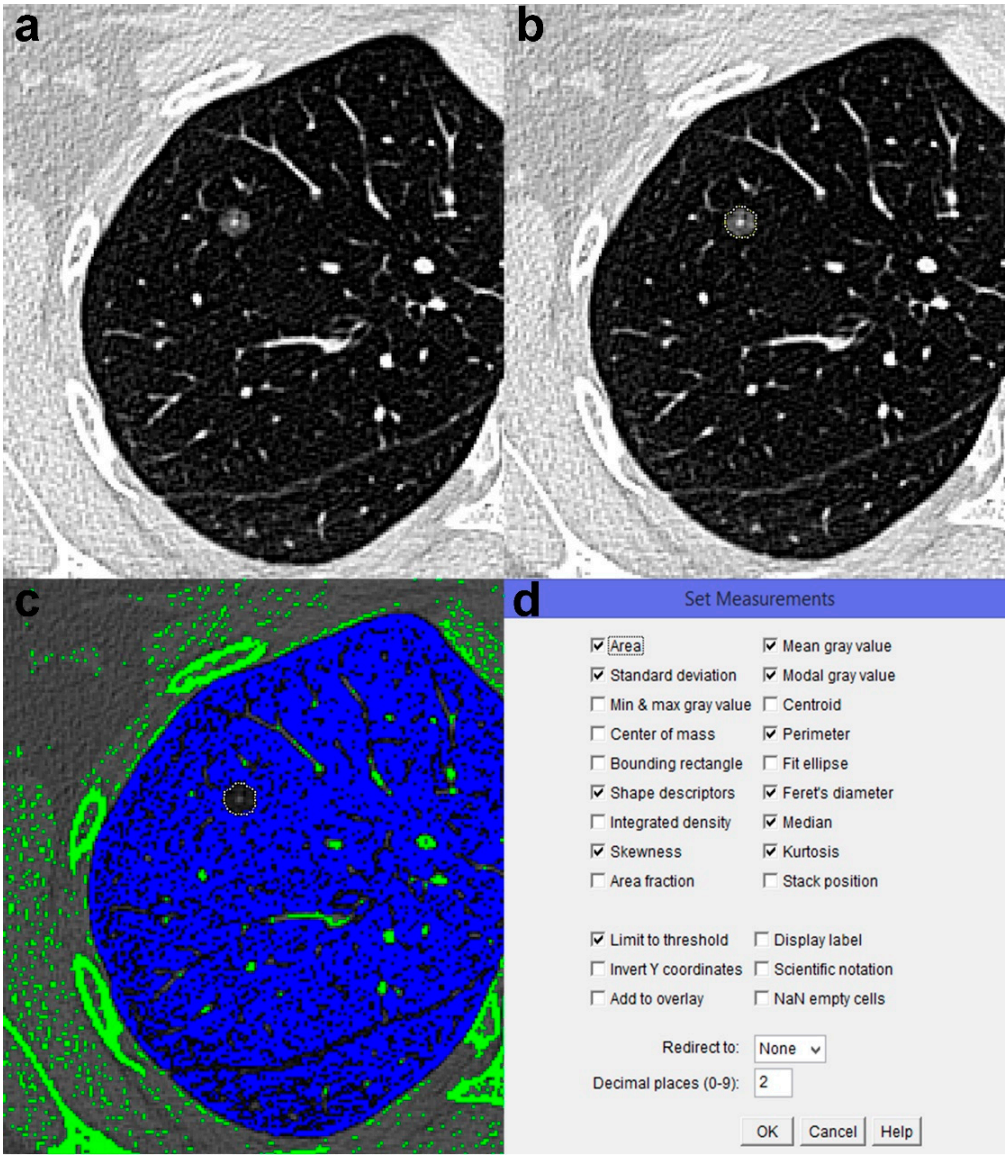

Figure 1. Example of segmentation process and computerized analysis performed using ImageJ software in a part-solid nodule (PSN). Step 1: importing the computed tomography (CT) images in DICOM format to ImageJ software (**a**). Step 2: drawing a polygonal region of interest (ROI) that outlined the nodule contours on the largest cross-sectional area of the lesion (**b**). Step 3: checking and manually correcting any segmentation error. Step 4: clicking "Image" on the ImageJ toolbar and selecting "Adjust → Threshold". Step 5: choosing a suitable CT attenuation value to excluded pixels with air attenuation around and within the PSNs (CT attenuation value, −800 HU) (**c**). Step 6: clicking "Analyze" on the toolbar, selecting "Set Measurement" and checking the quantitative features of interest (**d**). Step 7: clicking "Analyze" again and then clicking "Measure", to automatically calculate the selected quantitative features.

Since the segmentation was performed on only the largest cross-sectional area of the PSNs, the mass was not calculated [27,28]. As a viable alternative, we used the linear mass density (LMD), which was defined as the amount of mass per unit length. Typically, this quantitative feature is used to describe the characteristics of one-dimensional objects. However, the LMD may also be used to describe the density of a three-dimensional object along one particular dimension. Therefore, we considered the LMD to be adaptable for the quantitative analysis of PSNs. The LMD was calculated with the following Equation (1):

$$\text{LMD (mg/mm)} = [\text{Area} \times (\text{Mean CT Attenuation} + 1000)]/1000 \quad (1)$$

We also considered the following shape descriptors typically used in particle analysis: circularity and solidity [24–26].

Circularity is a dimensionless value that defines the degree to which a nodule resembles a circle [24–26]. The circularity value ranges between 0.0 and 1.0 [24–26]. A value of 1.0 corresponds to a perfect circle, whereas a circularity value approaching 0.0 defines a non-spherical shape (Figure 2) [24–26]. The equation for circularity (Equation (2)) is as follows [24]:

$$\text{Circularity} = 4\,\pi \times [\text{Area}]/[\text{Perimeter}]^2 \quad (2)$$

Solidity is also a dimensionless value that ranges between 0.0 and 1.0. This measurement represents the overall concavity of a nodule [24–26]. A solidity value of 1.0 indicates a very smooth nodule shape, whereas a value approaching 0.0 indicates an irregular nodule shape (Figure 2) [24–26]. The equation for solidity (Equation (3)) is as follows [24]:

$$\text{Solidity} = [\text{Area}]/[\text{Convex Area}] \quad (3)$$

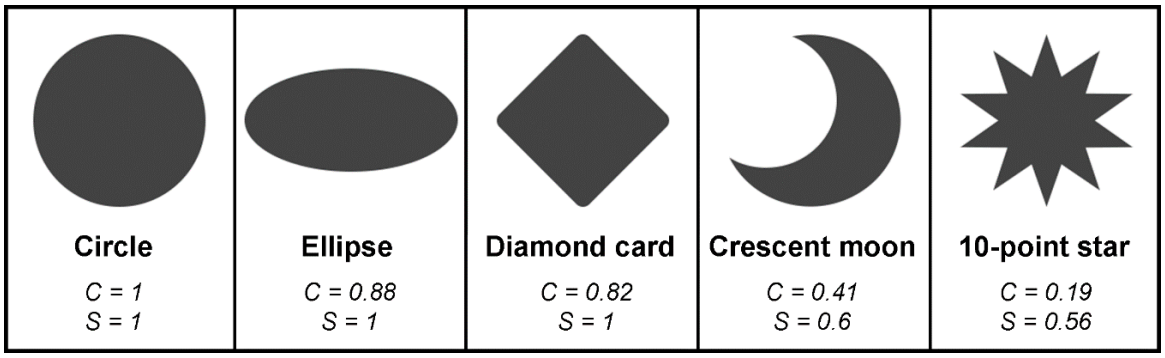

Figure 2. Image showing various shapes (circle, ellipse, diamond card, crescent moon, 10-point star) and their respective circularity (*C*) and solidity (*S*) values.

Subsequently, the segmentation process was also carried out on the last follow-up CT images; however, only the LMD was considered. These measurements were performed to quantify the growth of the PSNs by calculating the change in the LMD and the LMD-doubling time (LMD-DT).

The computerized analysis was performed by the most experienced thoracic radiologist (A.B.), who also had 8 years of experience using ImageJ software.

In addition, to determine the minimum positive variation in the LMD required to define nodule growth as significant, the LMD measurements for each PSN were repeated on the baseline CT images by the same thoracic radiologist after a time interval of at least one month. For each PSN, the minimum time interval required to detect growth (i.e., above the minimum positive LMD variation required to define the nodule growth as real) was also calculated.

All procedures performed in this study were in accordance with the Helsinki Declaration of 1975 and its later amendments. This study was approved and authorized by our local ethics committee (Ethics Committee of the Province of Brescia) as a retrospective analysis (Protocol No. 3435; 1 March 2019).

2.4. Statistical Analysis

The data are presented as the number (%) or the mean ± standard deviation for normally distributed data or as the median and interquartile range (IQR) for non-normally distributed data.

The Spearman rank correlation was applied to analyze correlations between the LMD-DT and the quantitative CT features (i.e., area, perimeter, mean, median, mode and standard deviation of CT

attenuation, skewness, kurtosis, mean Feret diameter, LMD, circularity and solidity). We applied this nonparametric test because the LMD-DT was not normally distributed.

Bland–Altman analysis was used to determine the minimum positive variation in the LMD required to define nodule growth as significant. In this analysis, the difference between the LMD measurements was defined as the percentage of the differences in each pair of measurements divided by the first LMD measurement. From the Bland–Altman analysis, we obtained the coefficient of repeatability (CR) [29], which was calculated as 1.96 times the standard deviation of the difference between the measurements. In other words, the CR provided a percentage value above which the PSN growth could be considered significant.

We also compared the quantitative CT features of growing and nongrowing PSNs using the Mann–Whitney U-test.

The chi-squared (χ^2) test was used to determine whether there were significant relationships between PSN growth and certain independent variables (such as patient age, sex, smoking habits, oncologic history, emphysema status and PSN lobe location). Multivariate analysis was also used to identify independent predictive variables of growth.

Statistical analysis was conducted with a dedicated software (MedCalc Software version 19, Ostend, Belgium, 2019), and a p value < 0.05 was considered statistically significant.

3. Results

Segmentation and computerized analysis with ImageJ software were successfully performed for all PSNs. The quantitative CT features calculated from the baseline CT images are listed in Table 2.

The time interval between the baseline and last follow-up CT scan ranged from 99 to 2224 days (median, 699 days; IQR, 263–1232 days). The LMD calculated from the last follow-up CT images ranged from 12.6 to 129.7 mg/mm (median, 42.4 mg/mm; IQR, 25.2–71.8 mg/mm). The LMD-DT calculated by matching the baseline and last follow-up CT images ranged from 343 to 25520 days (median, 1422 days; IQR, 1005–9018 days). A statistically significant correlation was observed between the LMD-DT and the quantitative CT features, including area, perimeter, mean Feret diameter, LMD, circularity and solidity ($p \leq 0.031$) (Table 2).

The CR obtained from the Bland–Altman analysis was 11.3% (Figure 3). Therefore, only an increase in the LMD greater than 11.3% was considered significant growth.

Table 2. Quantitative CT features calculated from the baseline CT images of all part-solid nodules.

CT Feature	Value	Spearman's Rho *	p Value *
Area (mm^2)	67 (40.5–86.8)	−0.306	0.031
Perimeter (mm)	36.9 (27.6–46.4)	−0.449	0.001
Mean Feret diameter (mm)	11 (8.3–13.2)	−0.365	0.009
Mean attenuation (HU)	−497.3 (−563.5–−449)	−0.069	0.633
Median attenuation (HU)	−534.5 (−605–−478)	−0.019	0.897
Modal attenuation (HU)	−703 (−758–−596)	−0.029	0.842
Standard deviation (HU)	226 (202.2–248.6)	−0.241	0.092
Skewness	0.67 (0.46–0.91)	−0.003	0.983
Kurtosis	−0.17 (−0.61–0.53)	0.124	0.390
LMD (mg/mm)	31.4 (20–43.5)	−0.326	0.021
Circularity	0.64 (0.52–0.75)	0.519	<0.001
Solidity	0.81 (0.74–0.87)	0.457	<0.001

* Spearman rank correlation between the quantitative features and the LMD doubling time. Data are presented as the median (interquartile range). LMD, linear mass density.

A significant increase in the LMD that exceeded the CR (i.e., >11.3%) between the baseline and last follow-up CT scan was detected in 33/50 (66%) PSNs. In this group of growing PSNs, the LMD increased from 12.3 to 235.2% (median, 55.4%; IQR, 30.9–89.9%) after a median time interval of 740 days (IQR, 340–1241 days) (Figure 4). The LMD-DT ranged from 343 to 5824 days (median, 1111 days;

IQR, 828–1520 days) with the minimum time interval needed to detect growth ranging from 40 to 880 days (median, 143 days; IQR, 101–217 days).

In this growing group, 12/33 (36.4%) PSNs were surgically removed with a histological diagnosis of pulmonary adenocarcinoma (nine minimally invasive adenocarcinomas graded as pT1mi and three invasive adenocarcinomas graded as pT1a). In 3/33 (9.1%) growing PSNs, stereotactic radiotherapy or radiofrequency ablation was performed due to the clinical status and comorbidities of the patients.

In the nongrowing group, which comprised 17/50 (34%) PSNs, the computerized analysis did not detect a significant change in the LMD after a median time interval of 349 days (IQR, 193–1026 days).

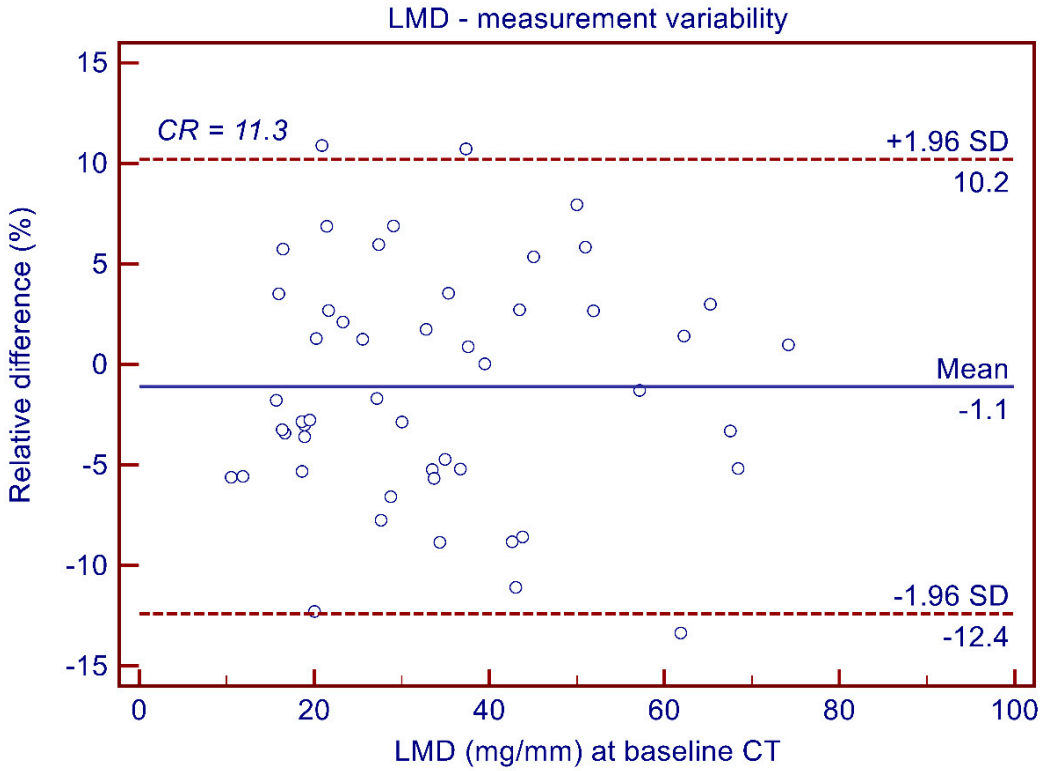

Figure 3. Bland–Altman plot showing the variability of the linear mass density (LMD) measurements. The mean difference in the LMD measurements is represented by the solid blue line. The upper and the lower limits of agreement are represented by the purple dashed lines. SD, standard deviation; CR, coefficient of repeatability.

The quantitative CT features that were significantly different between the groups of growing and nongrowing PSNs were area, perimeter, mean Feret diameter, standard deviation of CT attenuation, LMD, circularity and solidity ($p \leq 0.013$) (Table 3).

The relationships between PSN growth and independent variables (patient age, sex, smoking and oncologic history, emphysema status and PSN lobe location) were listed in Table 4.

Only oncologic history was significantly associated with PSN growth ($p = 0.004$). The relationship of nodule growth with sex ($p = 0.062$) and smoking history ($p = 0.061$) was just outside the limit of significance.

In multivariate analysis, oncologic history remained a significant independent variable associated with PSN growth (odds ratio, 7.2; 95% confidence interval, 1.72–29.98; $p = 0.007$).

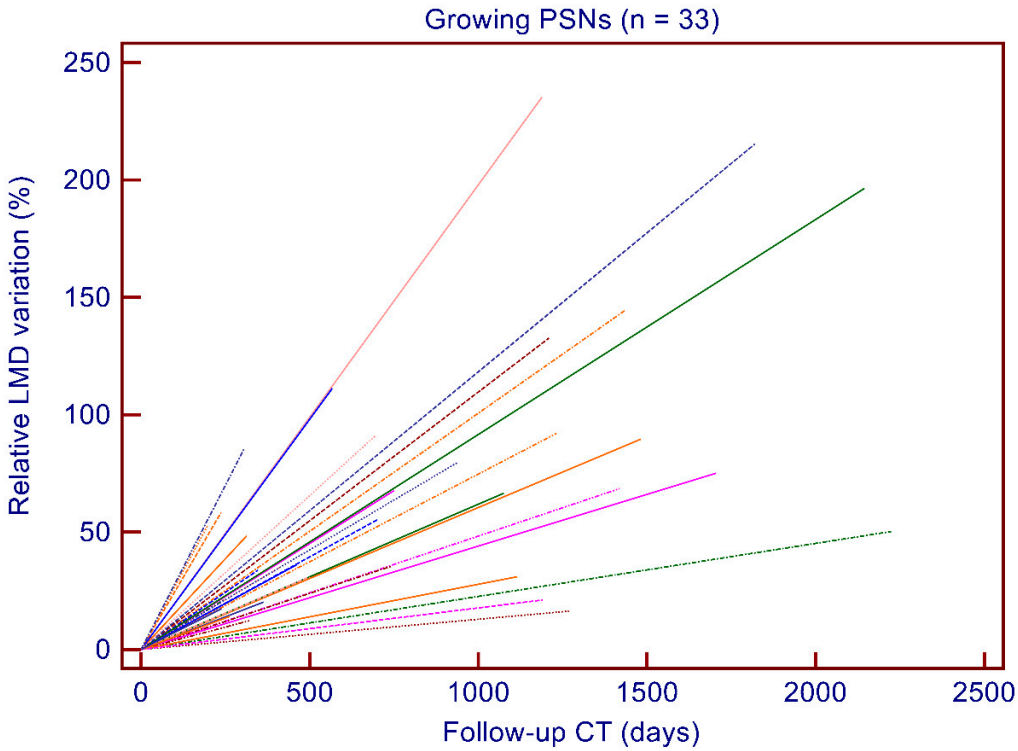

Figure 4. Growth pattern of the 33 growing part-solid nodules (PSNs) based on the linear mass density (LMD) changes during the follow-up CT scan.

Table 3. Quantitative CT features calculated from the baseline CT images of growing and nongrowing part-solid nodules (PSNs).

CT Feature	Growing PSNs	Nongrowing PSNs	*p* Value *
Area (mm^2)	76.7 (45.1–96.1)	45.6 (36.6–66.9)	0.008
Perimeter (mm)	42.5 (34.3–49.6)	30 (24.2–36.7)	<0.001
Mean Feret diameter (mm)	12.6 (9.4–13.7)	8.6 (7.6–10.7)	0.002
Mean attenuation (HU)	−490.5 (−551–−442.6)	−504.5 (−585.3–−455.6)	0.362
Median attenuation (HU)	−521 (−594.5–−476)	−548 (−618–−499)	0.566
Modal attenuation (HU)	−716 (−756.5–−647.5)	−674 (−765.0–−574)	0.401
Standard deviation (HU)	233 (204.4–255.9)	204.8 (188.8–225.3)	0.013
Skewness	0.7 (0.47–0.93)	0.67 (0.33–0.90)	0.846
Kurtosis	−0.33 (−0.59–0.29)	0.16 (−0.63–0.63)	0.676
LMD (mg/mm)	35.3 (22.8–44.2)	21.6 (18.1–30)	0.007
Circularity	0.59 (0.46–0.66)	0.76 (0.64–0.82)	<0.001
Solidity	0.78 (0.71–0.84)	0.88 (0.82–0.93)	0.001

* Mann–Whitney U-test. Data are presented as the median (interquartile range). LMD, linear mass density.

Table 4. Associations between part-solid nodule (PSN) growth and independent variables (patient age, sex, smoking history, oncologic history, emphysema status and PSN lobe location).

Independent Variables	PSN Outcome		χ^2 Test
	Growing (*n* = 33)	Nongrowing (*n* = 17)	*p* Value
Patient age			
≤65 years	14 (28)	10 (20)	0.276
>65 years	19 (38)	7 (14)	
Patient sex			
Male	19 (38)	5 (10)	0.062
Female	14 (28)	12 (24)	

Table 4. *Cont.*

Independent Variables	PSN Outcome		χ^2 Test
	Growing (n = 33)	Nongrowing (n = 17)	p Value
Smoking history			
No	7 (14)	8 (16)	0.061
Yes	26 (52)	9 (18)	
Oncologic history			
No	13 (26)	14 (28)	0.004
Yes	20 (40)	3 (6)	
Emphysema			
No	24 (48)	11 (22)	0.562
Yes	9 (18)	6 (12)	
Lobe location			
Middle/lower	10 (20)	8 (16)	0.247
Upper	23 (46)	9 (18)	

Data are presented as the number (percentage).

4. Discussion

Methods for the quantitative analysis of medical CT images are constantly expanding, and the applications of such methods in the thoracic field are increasing [4,5,9,14,17–22,28,30–34].

In clinical practice, quantitative CT analysis applications are most popular and most used for lung nodules [35,36]. Among the quantitative CT applications for lung nodules, those related to persistent SSNs have garnered the most interest from radiologists and clinicians in the last five years [9,14,17–22,37–41].

This particular interest in persistent SSNs is because in most cases, these lesions correspond to the preinvasive or invasive lepidic growth of pulmonary adenocarcinomas [9,20]. This statement was also confirmed by our study, in which all surgically removed PSNs corresponded to minimally invasive or invasive adenocarcinoma (nine minimally invasive adenocarcinoma and three invasive adenocarcinomas graded as pT1a).

Rarely, persistent SSNs may be the manifestation of benign lesions (organizing pneumonia/focal interstitial fibrosis) [42] or malignancies such as primitive pulmonary lymphomas [43] and pulmonary metastases from extrapulmonary malignancies [44].

Pulmonary adenocarcinomas presenting as SSNs exhibit heterogeneous growth patterns with a trend towards a progressive increase in size over time [9]. The literature reports that some lesions may grow rapidly, with a doubling time of less than one year, some may grow very slowly, with a doubling time of more than six years, and others may remain stable during follow-up [9]. These different growth patterns were also observed in our study, in which all 33 PSNs in the growing group exhibited different growth rates (Figure 4).

An indolent course with a very slow growth rate is most often observed in pure ground-glass nodules (PGGNs) and in PSNs with small solid components [14]. Therefore, surgical resection would not be recommended for all lesions of these SSN subtypes, as most of these SSNs will never become clinically relevant [7,8].

Moreover, PGGNs and PSNs with small solid components (especially those that are small in size) are often intraoperatively impalpable and indistinguishable from the normal parenchyma [45]; consequently, the localization of these nodules during video or robotic-assisted thoracoscopic surgery is very challenging without the use of a preoperative marking technique [45,46].

According to the new Fleischner Society guidelines [6], the management of solitary PSNs is mainly based on the size of the solid components, and an aggressive approach is justified only for lesions

with solid components ≥6 mm. As a result, for PSNs with a solid component <6 mm, conservative management is recommended [6,14].

From this point of view, appropriate knowledge about the growth patterns of solitary PSNs with small solid components is an important issue in lung cancer screening and in clinical practice.

The translation of morphological analysis from a visual to computerized assessment seems to be very promising for the management of SSNs, as this approach may help to predict the behavior of these nodules and consequently aid in the early detection of surgical and nonsurgical nodules.

Various quantitative CT features have been tested to predict the growth and improve the risk stratification of SSNs [9,14,17–22,37,38,47]. However, most of these studies have considered PGGNs [17–19,22,37,38] or SSNs without a distinction between PGGNs and PSNs [9,21].

To the best of our knowledge, this study is the first to perform quantitative CT analysis for predicting the behavior of PSNs with a solid component <6 mm and total diameter <15 mm. Our study is also the first to use shape descriptors (circularity and solidity) and the LMD for the quantitative CT analysis of SSNs.

Circularity and solidity were used to objectively define the nodule margins and the nodule shape. The LMD was used to accurately define the growth rate of PSNs during follow-up. The main advantage of the LMD is that this feature combines size and density measurements into a single value; therefore, we considered this feature appropriate for measuring changes in the SSNs on CT images, particularly when three-dimensional software is not available.

The present study demonstrates that the quantitative CT analysis performed with open-source image processing software was helpful for predicting the growth in a select group of PSNs with a solid component <6 mm and a total diameter <15 mm.

In particular, we found that the shape descriptors (circularity and solidity) and the size features (area, perimeter, mean Feret diameter, and LMD) were significantly correlated with LMD-DT and consequently with the growth rate of PSNs (Table 2). In addition, the same quantitative features showed statistical significance when we compared the groups of growing and nongrowing PSNs (Table 3). Therefore, the more irregular and nonspherical a PSN, the greater the likelihood of PSN growth (Figures 5 and 6). Additionally, this likelihood increases as the size of the PSN increases.

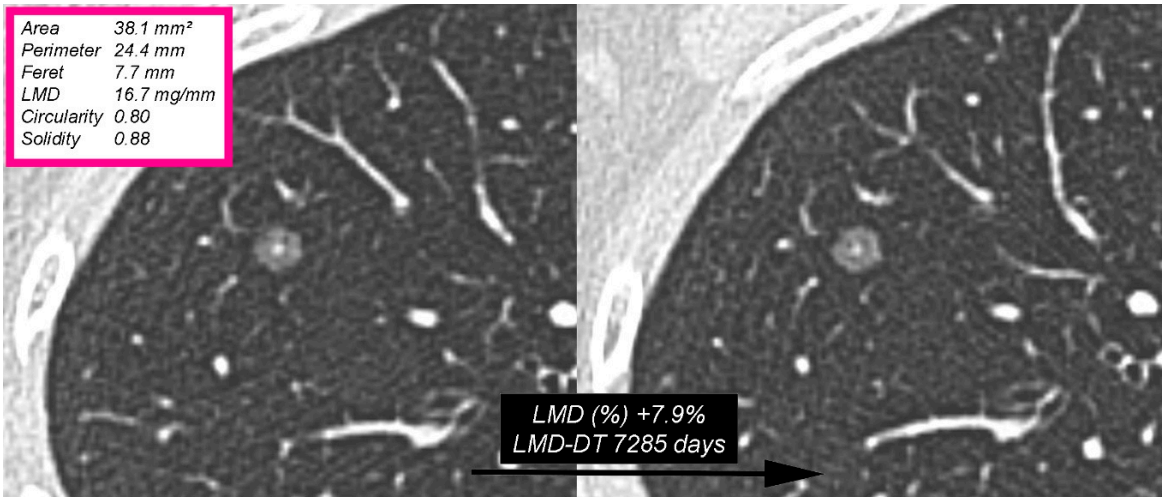

Figure 5. Nongrowing part-solid nodule (PSN) in the right upper lobe in a 43-year-old woman (nonsmoker and without an oncologic history). The PSN exhibits a rounded shape. The interval between the baseline (**left**) and last follow-up CT scan (**right**) was 789 days. The computerized analysis showed a relative linear mass density (LMD) variation of +7.9% in the nodule (less than the cut-off of 11.3%) with a LMD-doubling time (LMD-DT) of 7285 days. The purple box (top left) shows the main quantitative features obtained from the baseline CT image.

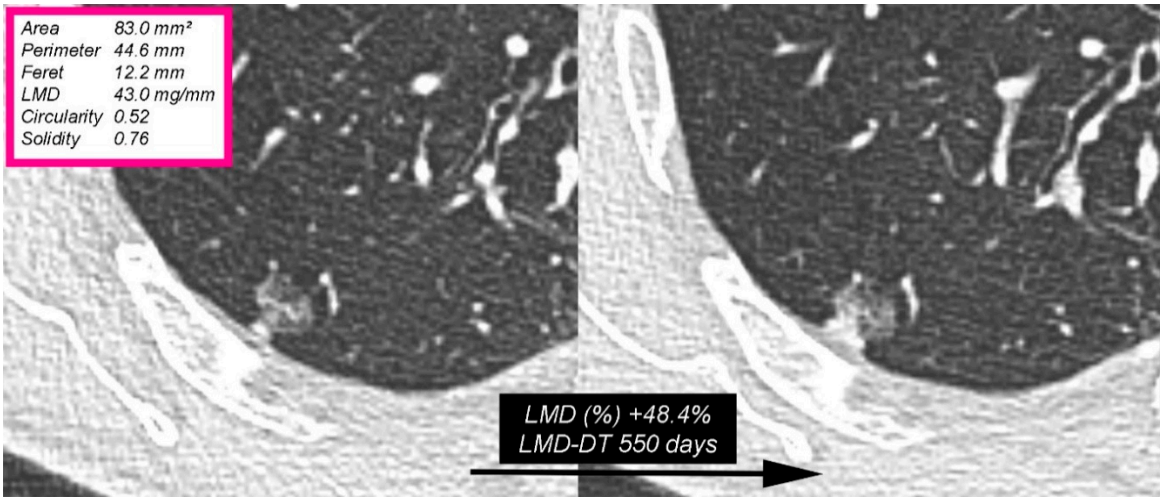

Figure 6. Growing part-solid nodule (PSN) in the right upper lobe in a 78-year-old man with a previous smoking and oncologic history. The PSN exhibits a mushroom shape. The interval between the baseline (**left**) and last follow-up CT scan (**right**) was 313 days. The computerized analysis showed a significant relative linear mass density (LMD) variation of +48.4% in the nodule with an LMD-doubling time (LMD-DT) of 550 days. The purple box (top left) shows the main quantitative features obtained from the baseline CT image.

No significant correlation was found between the LMD-DT and the quantitative features related to CT attenuation (mean, median, mode, standard deviation, skewness and kurtosis) (Table 2). No significant difference was also found in the density-related CT features (mean, median, mode, skewness and kurtosis) between the groups of growing and nongrowing PSNs.

In contrast to these results, data reported in the literature on PGGNs indicated that some density-related CT features could be helpful in predicting the future behavior of PGGNs [17–19,22]. This difference might be related to the different methods of analysis and SSN selection.

The only discrepancy observed in our data was related to the standard deviation of CT attenuation, which showed a statistically significant difference only when comparing the groups of growing and nongrowing PSNs (Table 3). However, we considered the nonsignificant correlation between the standard deviation and LMD-DT to be statistically more robust as the doubling time integrates information about both time and growth into a single value.

We also found that the median time interval to detect growth in the growing group was 143 days (IQR, 101–217 days). On the other hand, no significant change in the LMD was found in the nongrowing group after a median time interval of 349 days (IQR, 193–1026 days).

From a clinical point of view, we consider these results very interesting, as they could affect the guidelines for nodule management in terms of defining a "tailored" timing for the follow-up of PSNs with a small solid component. In addition, our quantitative analysis could be considered a useful diagnostic tool in the early discrimination between surgical and non-surgical PSNs.

We also found that the oncologic history was a significant independent variable for predicting the growth in PSNs with small solid components. Conversely, Lee et al. [11] reported that only lung cancer history was a significant predictive factor for growth in PSNs with a small solid component. This difference might be related to the different percentage of patients with a previous history of lung cancer (higher in our study).

Our study has some limitations. First, this study was retrospectively performed, and the time interval between the baseline and last CT follow-up scans was heterogeneous. Second, the number of PSNs selected was not large; however, the inclusion criteria were very strict, and only patients with a single PSN were included. Third, the computerized analysis was performed by one observer; however,

his experience in thoracic imaging and using ImageJ software may have improved the accuracy of the analysis.

5. Conclusions

This retrospective study found that in a select group of PSNs with a solid component <6 mm and diameter <15 mm, quantitative CT analysis was helpful for predicting the future behavior of nodules and improving risk stratification. In particular, the size features and shape descriptors calculated from the baseline CT images were significantly related to nodule growth. In addition, we found that oncologic history was a significant independent variable for predicting growth. We consider our quantitative CT analysis very promising in the management of PSNs with small solid components, as it could help in defining a "tailored" timing for the follow-up and consequently in the early detection of potentially surgical PSNs.

Author Contributions: Conceptualization, A.B.; data curation, A.B., A.S. and S.M.; formal analysis, A.B. and A.S.; investigation, A.B., A.S., G.C., S.G. and A.T.; methodology, A.B.; project administration, A.B. and R.M.; resources, A.B., A.S., G.C., S.G. and A.T.; validation, A.B.; writing–original draft, A.B., A.S. and S.M.; writing–review and editing, A.B., A.S., S.M., G.C, S.G., A.T. and R.M.

Funding: This research received no external funding.

Conflicts of Interest: The authors declare no conflict of interest.

References

1. Truong, M.T.; Ko, J.P.; Rossi, S.E.; Rossi, I.; Viswanathan, C.; Bruzzi, J.F.; Marom, E.M.; Erasmus, J.J. Update in the evaluation of the solitary pulmonary nodule. *Radiographics* **2014**, *34*, 1658–1679. [CrossRef] [PubMed]
2. Papapietro, V.R.; Milanese, G.; Borghesi, A.; Sverzellati, N.; Silva, M. Look around your target: A new approach to early diagnosis of lung cancer. *Ann. Transl. Med.* **2018**, *6*, S77. [CrossRef] [PubMed]
3. Larici, A.R.; Farchione, A.; Franchi, P.; Ciliberto, M.; Cicchetti, G.; Calandriello, L.; Del Ciello, A.; Bonomo, L. Lung nodules: Size still matters. *Eur. Respir. Rev.* **2017**, *26*, 170025. [CrossRef] [PubMed]
4. Borghesi, A.; Michelini, S.; Nocivelli, G.; Silva, M.; Scrimieri, A.; Pezzotti, S.; Maroldi, R.; Farina, D. Solid Indeterminate Pulmonary Nodules Less Than or Equal to 250 mm^3: Application of the Updated Fleischner Society Guidelines in Clinical Practice. *Radiol. Res. Pract.* **2019**, *2019*, 7218258. [CrossRef] [PubMed]
5. Borghesi, A.; Michelini, S.; Scrimieri, A.; Golemi, S.; Maroldi, R. Solid Indeterminate Pulmonary Nodules of Less Than 300 mm^3: Application of Different Volume Doubling Time Cut-offs in Clinical Practice. *Diagnostics* **2019**, *9*, 62. [CrossRef] [PubMed]
6. MacMahon, H.; Naidich, D.P.; Goo, J.M.; Lee, K.S.; Leung, A.N.C.; Mayo, J.R.; Mehta, A.C.; Ohno, Y.; Powell, C.A.; Prokop, M.; et al. Guidelines for Management of Incidental Pulmonary Nodules Detected on CT Images: From the Fleischner Society 2017. *Radiology* **2017**, *284*, 228–243. [CrossRef] [PubMed]
7. Kobayashi, Y.; Ambrogio, C.; Mitsudomi, T. Ground-glass nodules of the lung in never-smokers and smokers: clinical and genetic insights. *Transl. Lung Cancer Res.* **2018**, *7*, 487–497. [CrossRef]
8. Kobayashi, Y.; Mitsudomi, T. Management of ground-glass opacities: should all pulmonary lesions with ground-glass opacity be surgically resected? *Transl. Lung Cancer Res.* **2013**, *2*, 354–363.
9. Borghesi, A.; Farina, D.; Michelini, S.; Ferrari, M.; Benetti, D.; Fisogni, S.; Tironi, A.; Maroldi, R. Pulmonary adenocarcinomas presenting as ground-glass opacities on multidetector CT: Three-dimensional computer-assisted analysis of growth pattern and doubling time. *Diagn. Interv. Radiol.* **2016**, *22*, 525–533. [CrossRef]
10. Cohen, J.G.; Reymond, E.; Lederlin, M.; Medici, M.; Lantuejoul, S.; Laurent, F.; Arbib, F.; Jankowski, A.; Moreau-Gaudry, A.; Ferretti, G.R. Differentiating pre- and minimally invasive from invasive adenocarcinoma using CT-features in persistent pulmonary part solid nodules in Caucasian patients. *Eur. J. Radiol.* **2015**, *84*, 738–744. [CrossRef]
11. Lee, J.H.; Park, C.M.; Lee, S.M.; Kim, H.; McAdams, H.P.; Goo, J.M. Persistent pulmonary subsolid nodules with solid portions of 5 mm or smaller: Their natural course and predictors of interval growth. *Eur. Radiol.* **2016**, *26*, 1529–1537. [CrossRef] [PubMed]

12. Liu, Y.; Yankelevitz, D.F.; Kostakoglu, L.; Beasley, M.B.; Htwe, Y.; Salvatore, M.M.; Yip, R.; Henschke, C.I. Updating the role of FDG PET/CT for evaluation of lung cancer manifesting in nonsolid nodules. *Clin. Imaging* **2018**, *52*, 157–162. [CrossRef] [PubMed]
13. Kazerooni, E.A.; Austin, J.H.M.; Black, W.C.; Dyer, D.S.; Hazelton, T.R.; Leung, A.N.; McNitt-Gray, M.F.; Munden, R.F.; Pipavath, S. ACR-STR practice parameter for the performance and reporting of lung cancer screening thoracic computed tomography (CT): 2014 (Resolution 4). *J. Thorac. Imaging* **2014**, *29*, 310–316. [CrossRef]
14. Song, Y.S.; Park, C.M.; Park, S.J.; Lee, S.M.; Jeon, Y.K.; Goo, J.M. Volume and mass doubling times of persistent pulmonary subsolid nodules detected in patients without known malignancy. *Radiology* **2014**, *273*, 276–284. [CrossRef] [PubMed]
15. Lee, J.H.; Park, C.M.; Kim, H.; Hwang, E.J.; Park, J.; Goo, J.M. Persistent part-solid nodules with solid part of 5 mm or smaller: Can the 'follow-up and surgical resection after interval growth' policy have a negative effect on patient prognosis? *Eur. Radiol.* **2017**, *27*, 195–202. [CrossRef] [PubMed]
16. Gould, M.K.; Donington, J.; Lynch, W.R.; Mazzone, P.J.; Midthun, D.E.; Naidich, D.P.; Wiener, R.S. Evaluation of Individuals with Pulmonary Nodules: When is it Lung Cancer? Diagnosis and Management of Lung Cancer, 3rd ed.; American College of Chest Physicians evidence-based clinical practice guidelines. *Chest* **2013**, *143*, e93S–e120S. [CrossRef] [PubMed]
17. Tamura, M.; Shimizu, Y.; Yamamoto, T.; Yoshikawa, J.; Hashizume, Y. Predictive value of one-dimensional mean computed tomography value of ground-glass opacity on high-resolution images for the possibility of future change. *J. Thorac. Oncol.* **2014**, *9*, 469–472. [CrossRef] [PubMed]
18. Eguchi, T.; Kondo, R.; Kawakami, S.; Matsushita, M.; Yoshizawa, A.; Hara, D.; Matsuoka, S.; Takeda, T.; Miura, K.; Agatsuma, H.; et al. Computed tomography attenuation predicts the growth of pure ground-glass nodules. *Lung Cancer* **2014**, *84*, 242–247. [CrossRef]
19. Bak, S.H.; Lee, H.Y.; Kim, J.H.; Um, S.W.; Kwon, O.J.; Han, J.; Kim, H.K.; Kim, J.; Lee, K.S. Quantitative CT Scanning Analysis of Pure Ground-Glass Opacity Nodules Predicts Further CT Scanning Change. *Chest* **2016**, *149*, 180–191. [CrossRef]
20. Borghesi, A.; Michelini, S.; Bertagna, F.; Scrimieri, A.; Pezzotti, S.; Maroldi, R. Hilly or mountainous surface: A new CT feature to predict the behavior of pure ground glass nodules? *Eur. J. Radiol. Open* **2018**, *5*, 177–182. [CrossRef]
21. Sun, Q.; Huang, Y.; Wang, J.; Zhao, S.; Zhang, L.; Tang, W.; Wu, N. Applying CT texture analysis to determine the prognostic value of subsolid nodules detected during low-dose CT screening. *Clin. Radiol.* **2019**, *74*, 59–66. [CrossRef] [PubMed]
22. Shi, Z.; Deng, J.; She, Y.; Zhang, L.; Ren, Y.; Sun, W.; Su, H.; Dai, C.; Jiang, G.; Sun, X.; et al. Quantitative features can predict further growth of persistent pure ground-glass nodule. *Quant. Imaging Med. Surg.* **2019**, *9*, 283–291. [CrossRef] [PubMed]
23. Schneider, C.A.; Rasband, W.S.; Eliceiri, K.W. NIH Image to ImageJ: 25 years of image analysis. *Nature Methods* **2012**, *9*, 671–675. [CrossRef] [PubMed]
24. Rasband, W.S. ImageJ, U.S. National Institutes of Health, Bethesda, Maryland, USA, 1997–2018. Available online: https://imagej.nih.gov/ij/ (accessed on 11 March 2019).
25. Olson, E. Particle shape factors and their use in image analysis-Part 1: Theory. *J. GXP Compliance* **2011**, *15*, 85–95.
26. ISO. *ISO 9276-6:2008(E)—Representation of Results of Particle Size Analysis–Part 6: Descriptive and Quantitative Representation of Particle Shape and Morphology*; ISO: Geneve, Switzerland, 2008; pp. 1–23.
27. Mull, R.T. Mass estimates by computed tomography: Physical density from CT numbers. *AJR Am. J. Roentgenol.* **1984**, *143*, 1101–1104. [CrossRef] [PubMed]
28. de Hoop, B.; Gietema, H.; van de Vorst, S.; Murphy, K.; van Klaveren, R.J.; Prokop, M. Pulmonary ground-glass nodules: Increase in mass as an early indicator of growth. *Radiology* **2010**, *255*, 199–206. [CrossRef] [PubMed]
29. Bland, J.M.; Altman, D.G. Statistical methods for assessing agreement between two methods of clinical measurement. *Lancet* **1986**, *1*, 307–310. [CrossRef]
30. Ko, J.P.; Berman, E.J.; Kaur, M.; Babb, J.S.; Bomsztyk, E.; Greenberg, A.K.; Naidich, D.P.; Rusinek, H. Pulmonary Nodules: Growth rate assessment in patients by using serial CT and three-dimensional volumetry. *Radiology* **2012**, *262*, 662–671. [CrossRef] [PubMed]

31. Tantucci, C.; Bottone, D.; Borghesi, A.; Guerini, M.; Quadri, F.; Pini, L. Methods for Measuring Lung Volumes: Is There a Better One? *Respiration* **2016**, *91*, 273–280. [CrossRef]
32. Silva, M.; Milanese, G.; Seletti, V.; Ariani, A.; Sverzellati, N. Pulmonary quantitative CT imaging in focal and diffuse disease: Current research and clinical applications. *Br. J. Radiol.* **2018**, *91*, 20170644. [CrossRef]
33. Ravanelli, M.; Agazzi, G.M.; Ganeshan, B.; Roca, E.; Tononcelli, E.; Bettoni, V.; Caprioli, A.; Borghesi, A.; Berruti, A.; Maroldi, R.; et al. CT texture analysis as predictive factor in metastatic lung adenocarcinoma treated with tyrosine kinase inhibitors (TKIs). *Eur. J. Radiol.* **2018**, *109*, 130–135. [CrossRef] [PubMed]
34. Gawlitza, J.; Sturm, T.; Spohrer, K.; Henzler, T.; Akin, I.; Schönberg, S.; Borggrefe, M.; Haubenreisser, H.; Trinkmann, F. Predicting Pulmonary Function Testing from Quantified Computed Tomography Using Machine Learning Algorithms in Patients with COPD. *Diagnostics* **2019**, *9*, 33. [CrossRef] [PubMed]
35. Devaraj, A.; van Ginneken, B.; Nair, A.; Baldwin, D. Use of Volumetry for Lung Nodule Management: Theory and Practice. *Radiology* **2017**, *284*, 630–644. [CrossRef] [PubMed]
36. Goo, J.M. A computer-aided diagnosis for evaluating lung nodules on chest CT: The current status and perspective. *Korean J. Radiol.* **2011**, *12*, 145–155. [CrossRef] [PubMed]
37. Li, Q.; Fan, L.; Cao, E.T.; Li, Q.C.; Gu, Y.F.; Liu, S.Y. Quantitative CT analysis of pulmonary pure ground-glass nodule predicts histological invasiveness. *Eur. J. Radiol.* **2017**, *89*, 67–71. [CrossRef] [PubMed]
38. Nemec, U.; Heidinger, B.H.; Anderson, K.R.; Westmore, M.S.; VanderLaan, P.A.; Bankier, A.A. Software-based risk stratification of pulmonary adenocarcinomas manifesting as pure ground glass nodules on computed tomography. *Eur. Radiol.* **2018**, *28*, 235–242. [CrossRef]
39. Han, L.; Zhang, P.; Wang, Y.; Gao, Z.; Wang, H.; Li, X.; Ye, Z. CT quantitative parameters to predict the invasiveness of lung pure ground-glass nodules (pGGNs). *Clin. Radiol.* **2018**, *73*, 504.e1–504.e7. [CrossRef]
40. Zhang, Y.P.; Heuvelmans, M.A.; Zhang, H.; Oudkerk, M.; Zhang, G.X.; Xie, X.Q. Changes in quantitative CT image features of ground-glass nodules in differentiating invasive pulmonary adenocarcinoma from benign and in situ lesions: histopathological comparisons. *Clin. Radiol.* **2018**, *73*, 504.e9–504.e16. [CrossRef]
41. Fan, L.; Fang, M.; Li, Z.; Tu, W.; Wang, S.; Chen, W.; Tian, J.; Dong, D.; Liu, S. Radiomics signature: A biomarker for the preoperative discrimination of lung invasive adenocarcinoma manifesting as a ground-glass nodule. *Eur. Radiol.* **2019**, *29*, 889–897. [CrossRef]
42. Kim, H.Y.; Shim, Y.M.; Lee, K.S.; Han, J.; Yi, C.A.; Kim, Y.K. Persistent pulmonary nodular ground-glass opacity at thin-section CT: histopathologic comparisons. *Radiology* **2007**, *245*, 267–275. [CrossRef]
43. Albano, D.; Borghesi, A.; Bosio, G.; Bertoli, M.; Maroldi, R.; Giubbini, R.; Bertagna, F. Pulmonary mucosa-associated lymphoid tissue lymphoma: (18) F-FDG PET/CT and CT findings in 28 patients. *Br. J. Radiol.* **2017**, *90*, 20170311. [CrossRef] [PubMed]
44. Kang, M.J.; Kim, M.A.; Park, C.M.; Lee, C.H.; Goo, J.M.; Lee, H.J. Ground-glass nodules found in two patients with malignant melanomas: Different growth rate and different histology. *Clin. Imaging* **2010**, *34*, 396–399. [CrossRef] [PubMed]
45. Kim, H.; Park, C.M.; Koh, J.M.; Lee, S.M.; Goo, J.M. Pulmonary subsolid nodules: What radiologists need to know about the imaging features and management strategy. *Diagn. Interv. Radiol.* **2014**, *20*, 47–57. [CrossRef] [PubMed]
46. Abbas, A.; Kadakia, S.; Ambur, V.; Muro, K.; Kaiser, L. Intraoperative electromagnetic navigational bronchoscopic localization of small, deep, or subsolid pulmonary nodules. *J. Thorac. Cardiovasc. Surg.* **2017**, *153*, 1581–1590. [CrossRef] [PubMed]
47. Milanese, G.; Sverzellati, N.; Pastorino, U.; Silva, M. Adenocarcinoma in pure ground glass nodules: Histological evidence of invasion and open debate on optimal management. *J. Thorac. Dis.* **2017**, *9*, 2862–2867. [CrossRef] [PubMed]